Anomalous Temperature and Polarization Dependences of Photoluminescence of Metal-Organic Chemical Vapor Deposition-Grown $GeSe_2$

Eunji Lee, Krishna Prasad Dhakal, Hwayoung Song, Heenang Choi, Taek-Mo Chung, Saeyoung Oh, Hu Young Jeong, Juan Marmolejo-Tejada, Martín A. Mosquera, Dinh Loc Duong, Kibum Kang*, and Jeongyong Kim**

E. Lee., K. P. Dhakal, J. Kim
Department of Energy Science, Sungkyunkwan University, Suwon 16419, Republic of Korea
E-mail: j.kim@skku.edu

H. Song., K. Kang
Department of Materials Science and Engineering, Korea Advanced Institute of Science and Technology (KAIST), Daejeon 34141, Republic of Korea
E-mail: kibumkang@kaist.ac.kr

H. Choi, T. M. Chung
Thin Film Materials Research Center, Korea Research Institute of Chemical Technology, Daejeon 34114, Republic of Korea

S. Oh, H. Y. Jeong
Graduate School of Semiconductor Materials and Devices Engineering, Ulsan National Institute of Science and Technology (UNIST), Ulsan 44919, Republic of Korea

D. L. Duong
Department of Physics, Montana State University, Bozeman, Montana 59717, United States and MonArk NSF Quantum Foundry, Montana State University, Bozeman, MT 59717, United States
E-mail: dinhloc.duong@montana.edu

J. Marmolejo-Tejada, M. A. Mosquera
Department of Chemistry and Biochemistry, Montana State University, Bozeman, Montana 59717, United States and MonArk NSF Quantum Foundry, Montana State University, Bozeman, Montana 59717, United States

Keywords: MOCVD, $GeSe_2$, Se-vacancy, photoluminescence, polarization, 2D materials

Germanium diselenide ($GeSe_2$) is a two-dimensional (2D) semiconductor with air stability, a wide bandgap, and anisotropic optical properties. We studied the absorption and photoluminescence (PL) of single-crystalline 2D $GeSe_2$ grown by metal-organic chemical vapor deposition and their dependence on temperature and polarization. The PL spectra exhibited peaks at 2.5 eV (peak A) and 1.8 eV (peak B); peak A displayed a strongly polarized emission along the short axis of the crystal, and peak B displayed a weak polarization perpendicular to that of peak A. With increasing temperature, peak B showed anomalous behaviors, i.e., an increasing PL energy and intensity. The excitation energy-dependent PL, time-resolved PL, and a density functional theory calculation suggested that peak A corresponded to the band-edge transition, whereas peak B originated from the inter-band mid-gap states caused by the selenium vacancies passivated by oxygen atoms. Our comprehensive study on the PL of single-crystalline $GeSe_2$ sheds light on the origins of light emission in terms of the band structure of anisotropic $GeSe_2$, making it beneficial for the corresponding optoelectronic applications.

1. Introduction

The optical properties of two-dimensional (2D) layered materials have attracted considerable attention owing to their versatile uses in various optoelectronic applications such as polarization-dependent photodetectors, optical modulators, spin- and valley-dependent devices, and nano-mechanical devices.[1–8] The abundance of 2D isotropic and anisotropic lattice structures provide selectivity for use in a wide range of device applications.[1–14] Among them, germanium diselenide ($GeSe_2$) is a layered material representing a IV–VI chalcogenide with a wide bandgap. It exists in three phases: (a) orthorhombic α-$GeSe_2$, (b) monoclinic β-$GeSe_2$, and (c) hexagonal γ-$GeSe_2$.[1–3,8,15,16] β-$GeSe_2$ has shown excellent stability in air and adopts a monoclinic crystal structure with the $P2_1/c$ space group, exhibiting in-plane anisotropic, structural, vibrational, electrical, and optical properties.[1–3,8,9] Recent studies have shown that the wide (2.78 eV) bandgap of $GeSe_2$ has great potential for photodetector applications in the ultraviolet region.[1–3] Given its distinctive in-plane anisotropy, wide bandgap, and high air stability, $GeSe_2$ is a promising candidate for 2D optoelectronic applications.

$GeSe_2$ exhibits Raman modes with in-plane anisotropic characteristics under polarized light excitation;[1,3] these can be used to identify the crystal axis, similar to the case with other anisotropic 2D materials.[1,17] Photoluminescence (PL) studies on exfoliated bulk $GeSe_2$ have presented PL peaks at 2.78 and 1.55 eV.[2] The density functional theory (DFT) predictions for the electronic band structure attributed the high-energy gap (~2.8 eV) to the direct bandgap at the Γ point of the Brillouin zone, whereas the origin of the low-energy gap was not well-understood.[1–3] The calculated band structure showed a flat valance band structure without the signatures of indirect band gaps, i.e., emissions of $GeSe_2$.[1,2,8,16] Recently, Yan et al.[2] suggested that the low-energy peak (~1.55 eV) might be owing to a defect-related mid-gap state emission. In general, defect emissions are stronger at low temperatures and can be controlled by experimentally modifying the density of the defects.[5,14] One approach of modifying the density of defects is a plasma treatment. This treatment increases the density of the defects and consequently enhances the defect-induced PL emissions.[10] Furthermore, in anisotropic 2D lattices such as ReS_2 (Rhenium disulfide), band-edge excitons couple with a defect state to generate a neutral donor-bound exciton, demonstrating a linearly dichroic feature.[11] β-$GeSe_2$ is a candidate anisotropic 2D material; thus, investigating the characteristics of the PL, absorption, Raman spectra, temperature, and polarization dependency could provide crucial information regarding the origin of the different transitions

in the electronic and vibrational states.[11,12,18] However, no detailed understanding presently exists concerning the origins of the PL and absorption peaks in the electronic band structure of $GeSe_2$ and their dependencies on temperature and polarization.

In this study, we performed temperature- and polarization-dependent PL spectroscopy of 2D single-crystalline $GeSe_2$ grown using metal-organic chemical vapor deposition (MOCVD). We identified two distinct PL peaks at 2.5 and 1.8 eV. Based on the dependency on temperature, polarization, excitation energy, and DFT calculations, these peaks were attributed to the band-edge transition and mid-gap states owing to oxygen (O)-passivated selenium vacancies, respectively. Our comprehensive optical study provides crucial insights into the optical transitions of anisotropic $GeSe_2$, potentially benefitting the many optoelectronic applications using 2D $GeSe_2$.

2. Result and Discussions

2.1. Growth of $GeSe_2$

Figure 1a shows a schematic of the MOCVD for the growth of 2D $GeSe_2$. Bis(1-dimethylamino-2-methyl-2-propoxy) germanium (II) [$Ge(dmamp)_2$] and dimethyl selenide [$(CH_3)_2Se$] were used as the germanium (Ge) and selenium (Se) precursors, respectively. The first heating zone was heated to 480 °C for the precursor decomposition, and a muscovite mica substrate was placed in a second heating zone heated to 400 °C. As shown in Figure 1b, rhombic $GeSe_2$ flakes were uniformly distributed on the substrate. Atomic force microscopy further confirmed their rhombic shape and sharp facets (Figure 1c). The thickness of the as-grown flakes varied from 20 to 70 nm; the thickness distribution of 89 randomly selected $GeSe_2$ flakes is presented in the Supporting Information (Figure S1). X-ray diffraction (XRD) and transmission electron microscopy (TEM) analyses confirmed that the grown material was $GeSe_2$ (high-resolution TEM (HRTEM) in Figure S2). Figure 1d shows the XRD pattern of the rhombic flakes. The peaks matched well with those of monoclinic $GeSe_2$ (JCPDS-01-0710177). Only the (001) family peaks displayed alignment in the c-axis direction. Figure 1e shows a low-magnification TEM image of a rhombic flake. The corresponding selected area electron diffraction (SAED) pattern in Figure 1f shows sharp diffraction spots, indicating single crystals. The inter-layer d-spacings of 3.529 and 8.411 Å correspond to the (200) and (020) directions, respectively, consistent with the inter-layer d-spacing of $GeSe_2$.[19] Figure 1e and Figure 1f indicate that the long edges of the $GeSe_2$ flakes are in the [010] direction.

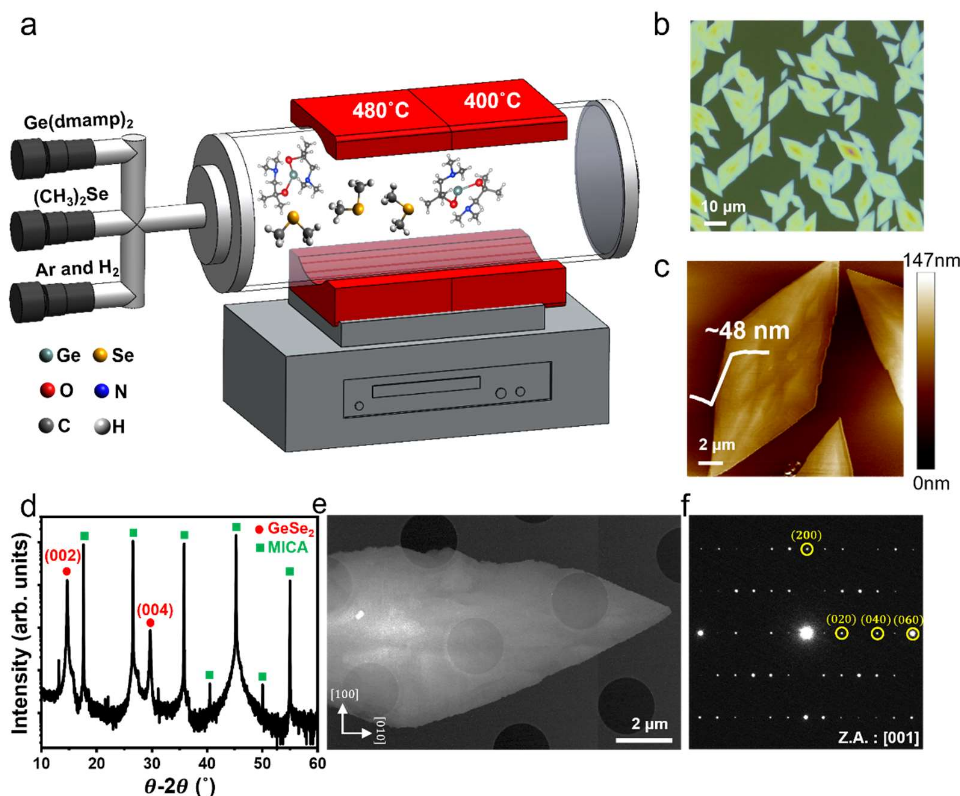

Figure 1. Growth and characterization of $GeSe_2$. a) Schematic of the metal-organic chemical vapor deposition (MOCVD) method for $GeSe_2$ growth. b) Optical image of rhombic $GeSe_2$ flakes on muscovite mica substrate. c) Atomic force microscopy image of $GeSe_2$ flakes. The inset shows the height of the flake. d) X-ray diffraction (XRD) pattern of $GeSe_2$. e) Low-magnification transmission electron microscopy (TEM) image of $GeSe_2$ flake and f) corresponding selected area electron diffraction (SAED) pattern.

2.2. Basic optical properties of $GeSe_2$

Figure 2a displays the representative Raman spectrum of the MOCVD-grown rhombohedral flakes of the $GeSe_2$ single crystals. We observe three distinct Raman modes at 96, 116, and 210 cm^{-1}, in agreement with previously reported results.[1,3,7,20,21] The most prominent peak is at 210 cm^{-1}; this is known as the A_g mode of $GeSe_2$.[1,3] The absence of the Raman mode at 200 cm^{-1} indicated that our MOCVD-grown $GeSe_2$ is a β-phase element.[1,3,21] The a- and b-axes in the rhombic flake are defined in reference to a unit cell of $GeSe_2$, as shown in the schematic lattice structure (top panel of Figure 2b). The polarization-dependent Raman spectra and polar plot of the A_g Raman mode at 210 cm^{-1} are shown in Figure S3 and Figure 2c, respectively, with 0° (and 180°) representing the polarization direction of the incident

light along the main crystal axis (b-axis) of $GeSe_2$ as shown in the optical image (bottom panel of Figure 2b). The bi-fold symmetry of the polarized Ratmdman intensity is consistent with the previously reported Raman anisotropy of $GeSe_2$.[1,3]

Optical micrographs of $GeSe_2$ with thicknesses of 76 and 131 nm are shown in Figure 2d, respectively (see Figure S4 for atomic force microscope measurement results). $GeSe_2$ is known for the weak interlayer coupling among 2D transition metal dichalcogendies (TMDs), the bandgap remaining direct,[2,8] thus the optical properties of these bulk thickness $GeSe_2$ can provide the representative characteristics of $GeSe_2$. The optical absorption spectra (Figure 2e, left panels) display two absorption peaks at approximately 2.9 (A peak) and 1.8 eV (B peak), with an energy separation of 1.1 eV. The position of absorption peak A matches well with previous results for a bulk $GeSe_2$,[1,2] whereas the absorption B peak is firstly observed here. We also measured the PL spectra of the same $GeSe_2$ crystals, with the results shown on the right panels of Figure 2e, where the A and B PL peaks are observed at 2.5 and 1.8 eV, respectively. While the peak position of A PL peak is similar to the previous result from exfoliated $GeSe_2$, B peak showed somewhat higher energy than the previous study.[2] This discrepancy is likely to originate from the difference in growth methods that can populate the different type or density of lattice defects. We are discussing later the origins of B peak and the lower energy shoulder peak (assigned as D peak) .

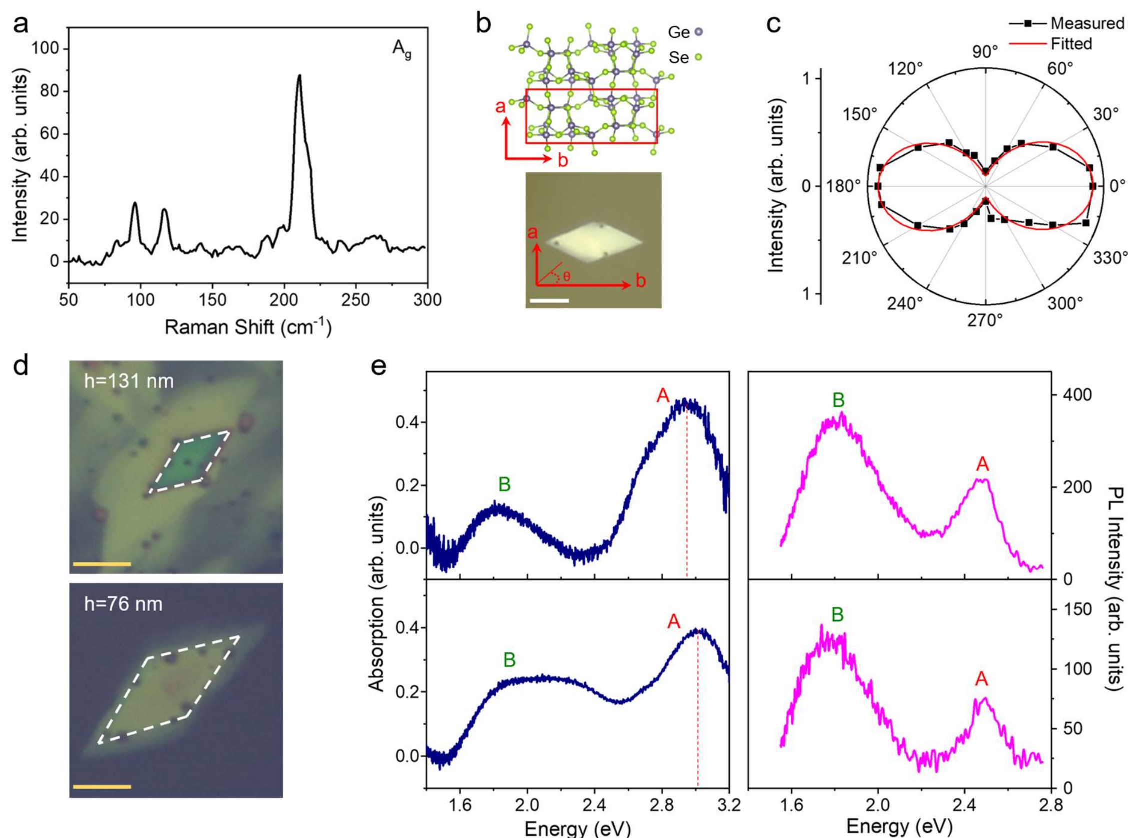

Figure 2. Anisotropic Raman properties, optical absorption, and photoluminescence (PL) emission of the 2D $GeSe_2$. a) Representative Raman spectrum of the 2D $GeSe_2$. A_g mode at 210 cm^{-1} was the most prominent. b) Top view of the lattice structure of the $GeSe_2$ (top panel) and optical view of the MOCVD-grown $GeSe_2$ (bottom panel). The unit cell of the $GeSe_2$ is represented by the rectangular box, and the crystalline axes are indicated by the a- and b-axes. The angle θ represents the incident polarization angle with respect to the b-axis. Scale bar represents 5 μm. c) Polarization polar plot of the Raman peak of A_g mode at 210 cm^{-1}. Scattered rectangles represent the measured data, and the solid trace is the fitted curve using the Raman tensor of $GeSe_2$.[1,3] d) Optical views of $GeSe_2$ samples used for the absorption and PL spectroscopy. Measured thickness (h) are shown. Scale bar represents 5 μm. e) Absorption spectra (left panels) and PL spectra (right panels) were obtained from the same samples (top panels and bottom panels). Two prominent PL and absorption peaks (A and B) are observed.

2.3. Temperature and polarization dependences of $GeSe_2$ PL

Figure 3a shows the temperature-dependent PL spectra of the $GeSe_2$ crystal (thickness of 76 nm) in the temperature range of 3–300 K. The PL spectra are normalized and vertically

shifted for clarity. We de-convolute the PL spectra with three PL peaks labeled as A, B, and D. The plots of the peak energy vs. temperature for these PL peaks are shown in Figure 3b; the error bars represent the standard deviations obtained for the three samples (the respective PL spectra of the other two samples are provided in Figure S5). With increasing temperature, the energies of peak A and peak B decrease and increase, respectively, whereas peak D remains largely unchanged. The observed red shift of peak A with an increasing temperature is consistent with the temperature dependence of the main exciton peak of other 2D semiconductors with direct band gaps.[14,18] This is owing to the thermally renormalized peak energy of the typical direct gap transition at the Γ point. The different temperature dependencies of peaks B and D indicate that they have different origins, such as phonon-assisted emissions or inter-band transitions.[2,18,22,23] To further understand the origin of peak B, we plotted the intensity ratio (I_B/I_A) as a function of the temperature (Figure 3c). The results reveal that the relative intensity of peak B gradually increases as the temperature increases, suggesting the phonon-assisted recombination of the B peak, similar to the indirect transition in multi-layer TMDs such as MoS_2 and WS_2.[18] Furthermore, when the energy difference between A and B peak continuously decreases with increasing temperature; this could expedite the phonon-assisted carrier transfer to the lower energy band, consequently amplifying the PL emissions of the B peak. In contrast, peak D is distinct at low temperatures but gradually decreases as the temperature increases (Plots of D peak intensity vs. tempertature of three $GeSe_2$ samples are provided in Figure S6). This is a common feature of the emissions from defects for most 2D TMD crystals.[18,22,23]

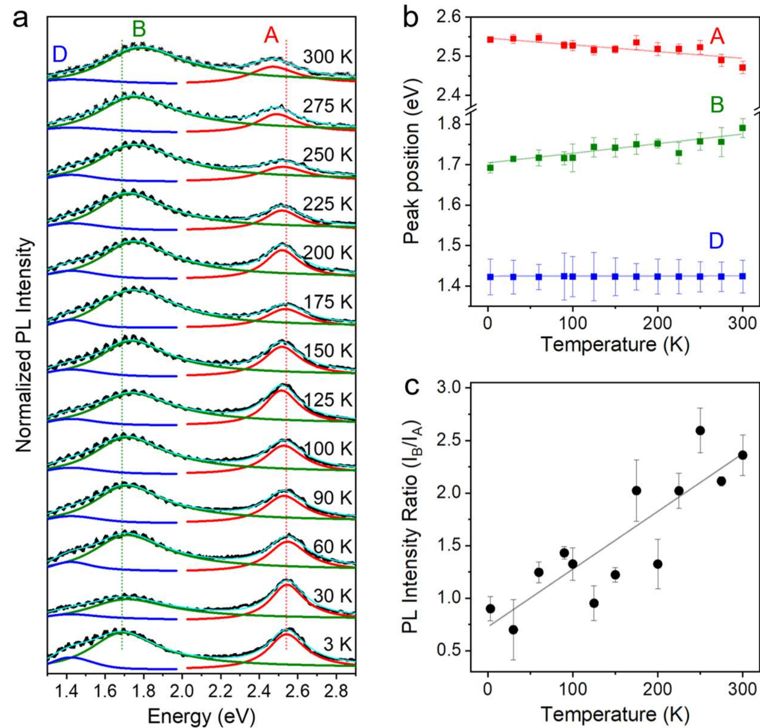

Figure 3. Temperature-dependent PL spectra. a) PL spectra obtained at various temperatures. PL was excited and collected without the polarization control. Vertical dotted lines are the guides for eyes to show the gradual shifts of PL peaks with the increasing temperature. Periodic undulation of PL curves is the result of the optical interference owing to the thickness of $GeSe_2$ flake. b) Plot of PL peak position vs. temperature for peaks A, B, and D, as identified by the multi-peak fitting process. Error bars are the standard deviations based on measurements taken for multiple samples. Linear fits (solid lines) show the decreasing and increasing trend of the energy of peaks A and B with the temperature, respectively. c) PL intensity ratio between peaks A and B ($\boldsymbol{I_B/I_A}$) as a function of temperature. Linear fit is shown as the solid line.

Polarization-dependent PL spectroscopy of the $GeSe_2$ crystals was performed at 3 K, and the results are shown in **Figure 4**. The rhombic flake of $GeSe_2$ was illuminated with a circularly polarized incident light, and the emission signal was collected by rotating a linear polarizer with 0° (and 180°) representing the direction of the main axis (b-axis) of the $GeSe_2$ crystal. On the detection side, we purposedly combined a quarter-wave plate and detection polarizer with the fixed angle of 45° and rotated them together so that the light entering the spectrometer is always circularly polarized to avoid the anisotropic responses of the spectrometer and charge-coupled device (CCD). A schematic of the setup for the polarized PL

measurements is shown in Figure 4a. We also performed a conventional polarization-dependent PL study where the input and output polarizers were aligned in parallel while the sample was rotated; similar results were obtained (Figure S7). The PL spectra as a function of the rotation angle of the linear polarizer are presented in Figure 4b, and the PL intensities of peaks A, B, and D, are plotted as polar plots in Figure 4c. Interestingly, peak A is polarized along the short axis (a-axis) of the $GeSe_2$ crystals, whereas peak B is polarized along the main axis (b-axis). We estimate the degree of polarization $(I_{max} - I_{min})/(I_{max} + I_{min})$ of peaks A and B to be 73 and 20 %, respectively. The strong polarization of the A peak of the 2D $GeSe_2$ is consistent with the PL characteristics of anisotropic 2D materials such as ReS_2 or $ReSe_2$,[11,12] suggesting that peak A results from the direct gap transition at the Γ point. In contrast, the broad PL peak width and relatively smaller degree of polarization of B peak suggests that peak B originates from the defect-induced states. Notably, peak D displays a non-polarized emission, indicating the origin of the typical defect states.

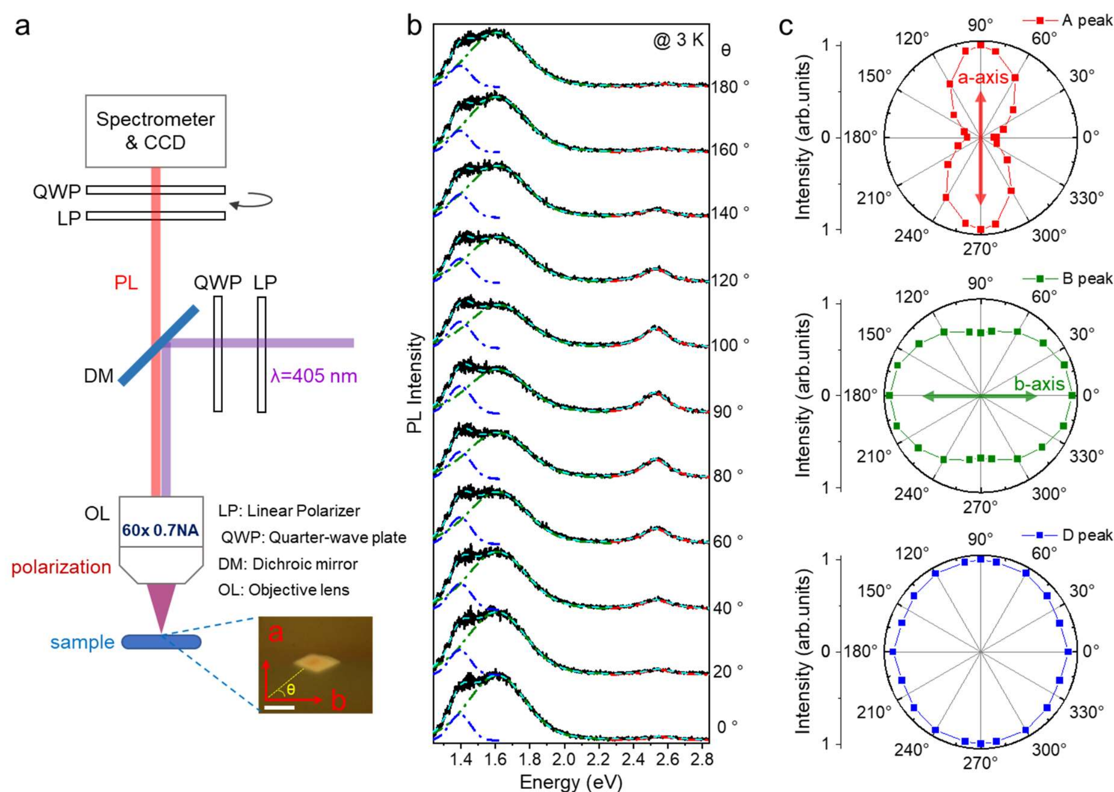

Figure 4. Mutually perpendicular polarization of PL peaks A and B. a) Schematic of the optical layout for the measurement of the polarization-dependent PL. The directions of crystalline a- and b-axes of the $GeSe_2$ are represented by the arrows in the optical view. Scale bar represents 5 μm. b) PL spectra obtained at various angles of the detection waveplate. c)

Polar plots of the intensities of peaks A, B, and D, as identified by multi-peak fitting. In polar plot, arrows are indicate the a- and b-axis direction, respectively.

2.4. Origin of $GeSe_2$ exciton peaks

We investigated the routes of photocarrier relaxation in $GeSe_2$ using different excitation laser energies corresponding to several energies with respect to the $GeSe_2$ absorption peaks. The laser energies used to excite the same $GeSe_2$ crystal are represented by dashed lines in the PL spectrum in **Figure 5**a (left panel), and the respective PL spectra are displayed in Figure 5a (right panel). For clarity, the PL spectra are vertically shifted and multiplied by appropriate factors. When the $GeSe_2$ sample is excited with 3.31 eV and 3.06 eV above the bandgap energy, comparable intensities of peaks A and B are observed in the PL spectra for A (dark blue and purple PL curves, respectively, Figure 5a). When decreasing the excitation energy to 2.54 eV, on-resonance energy of peak A or 2.33 eV, lower than the energy of peak A, but higher than that of peak B (1.8 eV), the PL intensity of B peak is strongly decrease and much weaker than that of A peak (blue and green curves in Figure 5a, respectively). An excitation energy of 1.96 eV in resonance with the PL peak B (1.8 eV) results in no discernible PL intensity (red curve in Figure 5a), indicating that PL peak B is detected only with an excitation energy higher than that of peak A. These results imply that peak A corresponds to the band-edge emission and the origin of peak B is the localized mid-gap states in the electronic structure of the $GeSe_2$.[2,22,23] The schematic in the inset of Figure 5a depicts the transitions of peaks A and B originating from the band edges and mid-gap states, respectively.

We also performed time-resolved PL (TRPL) with laser excitation at 3.31 eV and measured the relaxation times at PL peaks A and B. The normalized TRPL curves obtained from peaks A and B and the instrument response function are shown in Figure 5b. The PL decay curves are fitted with a bi-exponential decay for A peak and mono-exponential decay for B peak. The estimated average lifetime (t_{avg}) of peak B (823 ps) is distinctively longer than that of peak A (233 ps), again indicating the localized state of the peak B transition (Fitting parameters are given in Table S1 in Supporting Information).[24,25] Therefore, the broad PL spectrum, low degree of PL emission polarization, distinct temperature-dependent peak shift, and longer recombination lifetime could be attributed to the typical nature of the localized mid-gap states of 2D $GeSe_2$.

To help in identifying the origin of the PL peaks of $GeSe_2$, we performed X-ray photoemission spectroscopy (XPS). As shown in Figure 5c, the $GeSe_2$ exhibits two characteristic peaks at approximately 31 and 55 eV, corresponding to the doublet Ge 3d ($3d_{5/2}$, $3d_{3/2}$) and Se 3d ($3d_{5/2}$ and $3d_{3/2}$) of $GeSe_2$.[26,27] Interestingly, the spectral fitting clearly shows the presence of Ge-O peaks (orange color),[26,27] indicating the prevailing formation of Ge-O bonds in our MOCVD-fabricated $GeSe_2$. Considering that such oxidation should occur mostly from the $GeSe_2$ surface, we obtained the XPS patterns with an increasing argon (Ar) plasma treatment time. We found that the relative peak intensities of the Ge-O bonding decrease with the plasma treatment time, but the Ge-O peaks mostly maintain their intensities, suggesting that the Ge-O bonding prevails not only on the surface but also within the volumes of the $GeSe_2$ crystals (see Figure S8 for XPS spectra with different Ar plasma etching times). In addition, the XPS for the 1s O peak displays an additional peak at approximately 530.2 eV, attributed to the lattice O (Figure S8).[28] Notably, an O substitution in the chalcogenide vacancy is commonly observed in other 2D transition metal chalcogenide crystals.[29,30] Correspondingly, our XPS measurement also indicates O substitution at the Se vacancies in the $GeSe_2$ lattice.

Figure 5d (left panel) shows the electronic band structures (as calculated using DFT with PBE functional) of the bulk $GeSe_2$ (black line) and O substitution of the Se vacancies in the $GeSe_2$ (orange line) (details of scheme of molecular structures and their corresponding band structures are provided in Figure S9-S11 of Supporting Information). The fundamental direct bandgap at the Γ point is estimated as 1.41 eV for the $GeSe_2$, i.e., lower than the experimentally observed value (2.9 eV) but consistent with the previous DFT result for $GeSe_2$. Significant underestimations of the bandgap are frequently observed in DFT calculations using the PBE functional We have performed the band structure calculation with HSE06 functional (Supporting Information Fig. S12), which shows a band gap of 2.6 eV. Notably, the DFT calculation results with an O substitution of approximately 3% Se vacancies in $GeSe_2$ (orange color) shows that an additional mid-gap state is induced. The mid-gap states, owing to the presence of Se vacancies (a band structure with unsubstituted Se vacancies is provided in Figure S10), are fully converted into the band state with an O substitution, and the respective conduction band disperses from the Γ point to the U point. The DOS for Ge, Se, and O are also shown (right panel of Figure 5d). The A and B transitions are also assigned in the DOS plot of $GeSe_2$ with the O substitution at the Se vacancies (orange line). The available DOSs of O (p) at the conduction band are localized and orders of magnitude lower, indicating that the PL emission from the B peak will not be efficient unless the energy of the

photoexcitation is higher than that of the band-to-band A transition. This is consistent with the results from the excitation energy-dependent PL spectroscopy, as shown in Figure 5a. The results from our calculated electronic band structure and DOS strongly suggest that the transitions of A and B in the PL and absorption spectra can be attributed to the band gap of the $GeSe_2$ and mid-gap state transition, respectively, as indicated by the red and green arrows in Figure 5d (left panel). In DOS (right panel of Figure 5d), purple arrow indicates the band-edge PL corresponding to PL A peak, and dark blue arrow represents the absorption transition and the large shift of A peak energy by ~400 meV between the absorption and the PL is attributed to the large energy difference between the band edge and maximum density of states (DOS) of the conduction band of $GeSe_2$. In addition, the conduction band of the B peak has two valleys at the Γ and U points with an energy difference of 15 meV, implying the possibility of phonon-assisted transitions among different valleys.[18,31] Nevertheless, the nature of the indirect transition of the B peak is not clearly understood and requires further study. Notably, the slightly higher band gap at the Z point relative to that at the Γ point could be the cause of the broad spectral width in the observed absorption peak B (Figure 2e).

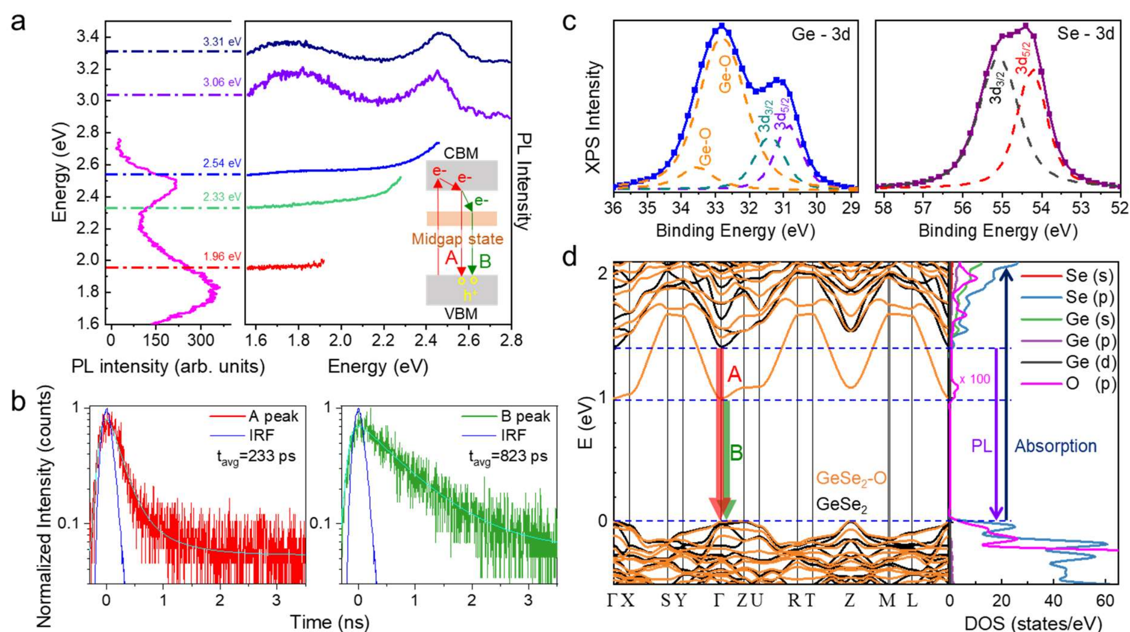

Figure 5. a) Typical $GeSe_2$ PL spectrum (left panel), where dashed lines indicate the energies of the excitation lasers used for PL spectroscopy. Respective PL spectra obtained at various laser excitation energies are shown in the right panel. The inset scheme indicates the band edge transition of peak A and the mid-gap states transition of peak B; VBM and CBM represent the valence band maxima and conduction band minima, respectively. b) Time-

resolved PL (TRPL) decay curves obtained from the PL emissions of peaks A and B, where the average lifetimes (t_{avg}) were estimated as 233 and 823 ps, respectively. Instrument response function (IRF) of the TRPL system is also shown. c) X-ray photoemission spectroscopy (XPS) spectra of the $GeSe_2$ for the core level orbitals of Ge and Se. The formation of the Ge-O boding is indicated by orange curves in the fitted result. d) Left panel: Density functional theory (DFT) calculation result of the electronic band structure of the bulk $GeSe_2$ with (orange line) and without (black line) oxygen (O) substituted Se vacancies. The red and green arrows at point Γ indicate the PL transition from the band edge (A peak) and the mid-gap state (B peak), respectively. Right panel: Calculated density-of-state (DOS) of Ge, Se, and O.

3. Conclusion

We showed that MOCVD-grown 2D $GeSe_2$ displayed a wide range of light absorption with two major exciton peaks at 2.95 eV (peak A) and 1.8 eV (peak B). Both peaks emitted PL with distinctively different polarizations. With increasing temperature, the energies of peaks A and B decreased and increased, respectively. The excitation-energy-dependent PL, TRPL, and DFT calculation results suggested that peak A originated from the direct gap at the Γ point, whereas peak B originated from the localized mid-gap states caused by the O substitution in the Se vacancies. Our results provide a comprehensive illustration of the origins of light emissions from 2D $GeSe_2$, paving the way for future optoelectronic applications using 2D $GeSe_2$.

4. Experimental Section

Synthesis of the $GeSe_2$ Crystal: The $GeSe_2$ was grown using the MOCVD method using a horizontal quartz tube with a diameter of 2 inches. Freshly cleaved muscovite mica was used as the growth substrate. $Ge(dmamp)_2$ and $(CH_3)_2Se$ were used as the Ge and Se precursors, respectively. The $Ge(dmamp)_2$ was stored in a canister kept at 45 °C and directly injected into the tube by flowing Ar gas. The $(CH_3)_2Se$ was maintained in a bubbler system at a constant pressure of 800 Torr. Ar was used as the carrier gas, with hydrogen gas (H_2) removing the carbon residue. The precise control of the flow rate was achieved using a mass flow controller. The optimized flow rates of the gas during growth were 60 sccm for $Ge(dmamp)_2$, 0.6 sccm for $(CH_3)_2Se$, 180 sccm for Ar, and 5 sccm for H_2. The furnace consisted of two heating zones; the precursors were decomposed in the first heating zone, and the material was grown in the second heating zone. The heating zones were heated to 480 and 400 °C for 30 minutes under 50 sccm Ar and 10 sccm H_2, respectively, with the temperature maintained during growth. The pressure was maintained at 300–400 Torr.

Structural characterizations: The XRD (SmartLab) patterns used Cu-Kα radiation to obtain the phase and crystallinity. The TEM analysis (Titan Cube G2 60-300, Thermo Fisher Scientific) was performed to obtain scanning TEM images, SAED patterns, and HRTEM images. Quantifoil carbon grids with 2 μm circular holes were used.

Optical measurements: The Raman and PL spectra were measured using a home-built optical setup in the inverted mode. A 100×, 0.95-numerical aperture (NA) objective lens was used to focus continuous laser light sources with different wavelengths (375, 405, 488, 532, and 633 nm). For low temperatures, we illuminated the sample with low laser power (~100 μW) to protect it from unintentional heating effects and obtained the PL and Raman spectra in the reflection geometry. The collected PL and Raman signals were guided to a 50-cm-long spectrometer equipped with a cooled CCD using an optical fiber with a core diameter of 105 μm. The Montana system (Cryostation s50) was used to obtain the temperature-dependent PL spectra using a 405-nm laser excitation between 3 and 300 K and a 60×, 0.7 NA objective lens. The optical absorption measurements were carried out using a home-built confocal microscope in the transmission mode,[13] wherein white light (tungsten source) was illuminated directly on the $GeSe_2$ nanoflake prepared on the transparent mica substrate.

Theoretical calculation: The electronic band structure of $GeSe_2$ was investigated based on DFT calculations. The exchange interactions between the electrons were estimated using the Perdew-Burke-Ernzerh of approximation function, performed employing the quantum Espresso code.[32,33] The potential of the core electrons was approximated using a projector-

augmented wave scheme with a cutoff energy of 40 Ry. A Monkhorst−Pack k-grid (8 × 3 × 5) was used to optimize the cell structure at a pressure and force of 0.5 kbar and 10^{-3} Ry/Bohr, respectively. The energy convergence for the self-consistent steps was 10^{-6} Ry.

HSE06 calculations: Electronic structure calculations were carried out using the LCAO (linear combination of atomic orbitals) method in density functional theory (DFT), as implemented in the QuantumATK package[1,2], where the Kohn-Sham (KS) Hamiltonian is represented in the basis of PseudoDojo pseudopotentials on all atoms[3], using a density mesh cut-off of 90 Hartree. We employed HSE06 hybrid functionals for the exact exchange contribution[4,5], an 8x3x5 Monkhorst−Pack grid for k-point sampling and a maximum tolerance difference of 5x10-5 for the self-consistent loop. All the structures were optimized for maximum force and stress of 0.05 eV/Å and 0.1 GPA, respectively.

[1] QuantumATK version S-2021.06-SP1, Synopsys QuantumATK (https://www.synopsys.com/silicon/quantumatk.html).
[2] S. Smidstrup, T. Markussen, P. Vancraeyveld, J. Wellendorff, J. Schneider, T. Gunst, B. Verstichel, D. Stradi, P. A. Khomyakov and U. G. Vej-Hansen, et al., J. Phys.: Condens. Matter, 2019, 32(1), 015901.
[3] M.J. van Setten, M. Giantomassi, E. Bousquet, M.J. Verstraete, D.R. Hamann, X. Gonze, and G.-M. Rignanese. The pseudodojo: training and grading a 85 element optimized norm-conserving pseudopotential table. Computer Physics Communications, 226:39 – 54, 2018.
[4] Heyd, J.; Scuseria, G. E.; Ernzerhof, M. Hybrid functionals based on a screened Coulomb potential. J. Chem. Phys. 2003, 118, 8207−8215.
[5] Heyd, J.; Scuseria, G. E.; Ernzerhof, M. Erratum: "Hybrid functionals based on a screened Coulomb potential" [J. Chem. Phys. 118, 8207 (2003)]. J. Chem. Phys. 2006, 124, 219906.

Supporting Information

Supporting Information is available from the Wiley Online Library or from the author.

Acknowledgements

J. Kim and K. P. Dhakal acknowledge financial support from the National Research Foundation of Korea (2021R1A6A1A03039696; 2022R1A2C2009412; 2022R1I1A1A01065580). K. Kang was supported by the National R&D Program through the National Research Foundation of Korea (NRF), funded by the Ministry of Science and ICT (2020M3D1A1110659, 2022M3H4A1A01010325). J. Marmolejo-Tejada., M.A. Mosquera, and D. L. Duong acknowledges support from the MonArk NSF Quantum Foundry supported by the National Science Foundation Q-AMASE-i program under NSF award DMR-1906383. Computational efforts were performed on the Tempest High Performance Computing System, operated and supported by University Information Technology Research Cyberinfrastructure at Montana State University. J.M.M.T. and M.A.M. thank Montana State University, Bozeman, for startup support and computational resources within the Tempest Research Cluster.

Author Contributions

E. Lee, K. P. Dhakal, and H. Song contributed equally to this work. J. Kim, K.P. Dhakal, and K. Kang planned the project. H. Song, H. Choi, T. M. Chung, and K. Kang synthesized the samples. E. Lee and K. P. Dhakal conducted the optical measurements and analyzed the data. S. Oh and H. Y. Jeong performed the TEM measurements. D. L. Duong performed theoretical calculations. E. Lee, K. P. Dhakal, H. Song, K. Kang, D. L. Duong and J. Kim wrote the manuscript. K. Kang and J. Kim supervised the project.

Received: ((will be filled in by the editorial staff))
Revised: ((will be filled in by the editorial staff))
Published online: ((will be filled in by the editorial staff))

References

[1] Y. Yang, S.-C. Liu, W. Yang, Z. Li, Y. Wang, X. Wang, S. Zhang, Y. Zhang, M. Long, G. Zhang, D.-J. Xue, J.-S. Hu, L.-J. Wan, *J. Am. Chem. Soc.* **2018**, *140*, 4150.

[2] Y. Yan, W. Q. Xiong, S. S. Li, K. Zhao, X. T. Wang, J. Su, X. H. Song, X. P. Li, S. Zhang, H. Yang, X. F. Liu, L. Jiang, T. Y. Zhai, C. X. Xia, J. B. Li, Z. M. Wei, *Adv. Opt. Mater.* **2019**, *7*, 1900622.

[3] X. Zhou, X. Hu, S. Zhou, Q. Zhang, H. Li, T. Zhai, *Adv. Funct. Mater.* **2017**, *27*, 1703858.

[4] S. Sim, D. Lee, A. V Trifonov, T. Kim, S. Cha, J. H. Sung, S. Cho, W. Shim, M.-H. Jo, H. Choi, *Nat. Commun.* **2018**, *9*, 351.

[5] M. Tripathi, F. Lee, A. Michail, D. Anestopoulos, J. G. McHugh, S. P. Ogilvie, M. J. Large, A. A. Graf, P. J. Lynch, J. Parthenios, K. Papagelis, S. Roy, M. A. S. R. Saadi, M. M. Rahman, N. M. Pugno, A. A. K. King, P. M. Ajayan, A. B. Dalton, *ACS Nano* **2021**, *15*, 2520.

[6] J. R. Schaibley, H. Yu, G. Clark, P. Rivera, J. S. Ross, K. L. Seyler, W. Yao, X. Xu, *Nat. Rev. Mater.* **2016**, *1*, 16055.

[7] A. S. Sharbirin, S. Akhtar, J. Kim, *Opto-Electronic Adv.* **2021**, *4*, 200077.

[8] Y. Yang, X. Wang, S.-C. Liu, Z. Li, Z. Sun, C. Hu, D.-J. Xue, G. Zhang, J.-S. Hu, *Adv. Sci.* **2019**, *6*, 1801810.

[9] K. Yumigeta, C. Brayfield, H. Cai, D. Hajra, M. Blei, S. Yang, Y. Shen, S. Tongay, *RSC Adv.* **2020**, *10*, 38227.

[10] Y. Liu, H. Nan, X. Wu, W. Pan, W. Wang, J. Bai, W. Zhao, L. Sun, X. Wang, Z. Ni, *ACS Nano* **2013**, *7*, 4202.

[11] C.-H. Ho, Z.-Z. Liu, *Nano Energy* **2019**, *56*, 641.

[12] O. B. Aslan, D. A. Chenet, A. M. van der Zande, J. C. Hone, T. F. Heinz, *ACS Photonics* **2016**, *3*, 96.

[13] K. P. Dhakal, D. L. Duong, J. Lee, H. Nam, M. Kim, M. Kan, Y. H. Lee, J. Kim, *Nanoscale* **2014**, *6*, 13028.

[14] M. S. Kim, S. J. Yun, Y. Lee, C. Seo, G. H. Han, K. K. Kim, Y. H. Lee, J. Kim, *ACS Nano* **2016**, *10*, 2399.

[15] M. Fuentes-Cabrera, H. Wang, O. F. Sankey, *J. Phys. Condens. Matter* **2002**, *14*, 9589.

[16] Z. Li, X. Wang, W. Shi, X. Xing, D.-J. Xue, J.-S. Hu, *RSC Adv.* **2018**, *8*, 33445.

[17] D. A. Chenet, O. B. Aslan, P. Y. Huang, C. Fan, A. M. van der Zande, T. F. Heinz, J. C. Hone, *Nano Lett.* **2015**, *15*, 5667.

[18] W. Zhao, R. M. Ribeiro, M. Toh, A. Carvalho, C. Kloc, A. H. Castro Neto, G. Eda, *Nano Lett.* **2013**, *13*, 5627.

[19] G. Dittmar, H. Schäfer, *Acta Crystallogr. Sect. B Struct. Crystallogr. Cryst. Chem.* **1976**, *32*, 2726.

[20] K. Inoue, O. Matsuda, K. Murase, *Solid State Commun.* **1991**, *79*, 905.

[21] K. Jackson, A. Briley, S. Grossman, D. V Porezag, M. R. Pederson, *Phys. Rev. B* **1999**, *60*, R14985.

[22] K. W. Acta Crystallographica Section BBöer, U. W. Pohl, in *Semicond. Phys.*, Springer International Publishing, Cham, **2018**, pp. 629–676.

[23] T. Verhagen, V. L. P. Guerra, G. Haider, M. Kalbac, J. Vejpravova, *Nanoscale* **2020**, *12*, 3019.

[24] S. Choi, M. R. Phillips, I. Aharonovich, S. Pornsuwan, B. C. C. Cowie, C. Ton-That, *Adv. Opt. Mater.* **2015**, *3*, 821.

[25] H. Shi, R. Yan, S. Bertolazzi, J. Brivio, B. Gao, A. Kis, D. Jena, H. G. Xing, L. Huang, *ACS Nano* **2013**, *7*, 1072.

[26] B. Mukherjee, Z. Hu, M. Zheng, Y. Cai, Y. P. Feng, E. S. Tok, C. H. Sow, *J. Mater. Chem.* **2012**, *22*, 24882.

[27] A. Prakash, S. Maikap, S. Z. Rahaman, S. Majumdar, S. Manna, S. K. Ray, *Nanoscale Res. Lett.* **2013**, *8*, 220.

[28] A. Ghosh, P. Guha, S. Mukherjee, R. Bar, S. K. Ray, P. V Satyam, *Appl. Phys. Lett.* **2016**, *109*, 123105.

[29] H. Shu, Y. Li, X. Niu, J. Wang, *ACS Appl. Mater. Interfaces* **2016**, *8*, 13150.

[30] S. Barja, S. Refaely-Abramson, B. Schuler, D. Y. Qiu, A. Pulkin, S. Wickenburg, H. Ryu, M. M. Ugeda, C. Kastl, C. Chen, C. Hwang, A. Schwartzberg, S. Aloni, S.-K. Mo, D. Frank Ogletree, M. F. Crommie, O. V Yazyev, S. G. Louie, J. B. Neaton, A. Weber-Bargioni, *Nat. Commun.* **2019**, *10*, 3382.

[31] S. Zhu, D. Li, Y. Hu, J. Wang, X. Wang, W. Lu, *Mater. Res. Express* **2018**, *5*, 066209.

[32] P. Giannozzi, O. Andreussi, T. Brumme, O. Bunau, M. Buongiorno Nardelli, M. Calandra, R. Car, C. Cavazzoni, D. Ceresoli, M. Cococcioni, N. Colonna, I. Carnimeo, A. Dal Corso, S. de Gironcoli, P. Delugas, R. A. DiStasio, A. Ferretti, A. Floris, G. Fratesi, G. Fugallo, R. Gebauer, U. Gerstmann, F. Giustino, T. Gorni, J. Jia, M. Kawamura, H. Y. Ko, A. Kokalj, E. Küçükbenli, M. Lazzeri, M. Marsili, N. Marzari, F. Mauri, N. L. Nguyen, H. V

Nguyen, A. Otero-de-la-Roza, L. Paulatto, S. Poncé, D. Rocca, R. Sabatini, B. Santra, M. Schlipf, A. P. Seitsonen, A. Smogunov, I. Timrov, T. Thonhauser, P. Umari, N. Vast, X. Wu, S. Baroni, *J. Phys. Condens. Matter* **2017**, *29*, 465901.

[33] J. Klimeš, D. R. Bowler, A. Michaelides, *Phys. Rev. B* **2011**, *83*, 195131.